Coupling optical and electrical gating for electronic readout of quantum dot dynamics

Smitha Vasudevan,[1] Kamil Walczak,[2] and Avik W. Ghosh[1]
[1]*Department of Electrical and Computer Engineering, University of Virginia, Charlottesville, Virginia 22904, USA*
[2]*Electronics Science & Technology Division, Naval Research Laboratory, Washington, DC 20375, USA*
(Received 22 November 2009; revised manuscript received 15 June 2010; published 25 August 2010)

We explore the coherent transfer of electronic signatures from a strongly correlated, optically gated nanoscale quantum dot to a weakly interacting, electrically backgated microscale channel. In this unique side-coupled "*T*" geometry for transport, we predict a mechanism for detecting Rabi oscillations induced in the dot through quantum, rather than electrostatic means. This detection shows up directly in the dc conductance-voltage spectrum as a field-tunable split in the Fano lineshape arising due to interference between the dipole coupled dot states and the channel continuum. The split is further modified by the Coulomb interactions within the dot that influence the detuning of the Rabi oscillations. Furthermore, time resolving the signal we see clear beats when the Rabi frequencies approach the intrinsic Bohr frequencies in the dot. Capturing these coupled dynamics requires attention to memory effects and quantum interference in the channel as well as many-body effects in the dot. We accomplish this coupling by combining a Fock-space master equation for the dot dynamics with the phase-coherent, non-Markovian time-dependent nonequilibrium Green's function transport formalism in the channel through a properly evaluated self-energy and a Coulomb integral. The strength of the interactions can further be modulated using a backgate that controls the degree of hybridization and charge polarization at the transistor surface.

DOI: 10.1103/PhysRevB.82.085324 PACS number(s): 73.63.−b, 42.50.Hz, 73.23.Hk, 85.35.−p

Future electronic devices are likely to contain nanoscale components ranging from random traps, defects and dopants, to engineered memories, logic elements and sensors. For practical reasons, these elements must interface with a larger microsystem, such as contacts and substrates. The rapidly increasing surface sensitivity will make ultimately scaled device properties strongly dependent on the dynamics and low-frequency noise generated by these nanoscale components.[1] The issue of how the nanodomains and microdomains "talk" to each other lies at the very heart of the operation of tomorrow's electronics.

The dynamics of electrons in dots and channels are significantly different due to the distinct energy scales involved. Inside larger transport channels where electronic interactions are screened, it is traditional to solve the *one-electron* Schrödinger equation (Fig. 1, left) with nonequilibrium thermal boundary conditions, treating electron-electron interactions as a mean field. The consequent perturbative nonequilibrium Green's function formalism[2,3] has been successful in quantitatively describing current flow through systems as diverse as molecular wires, carbon nanotubes, silicon nanowires, and spintronic systems. The operating regime is often described by the inequality $U_0 \ll \Gamma$, where U_0 is the single-electron charging energy and Γ is the level broadening. In contrast, strong confinement of electrons in quantum dots ($U_0 \gg \Gamma$) amplifies their many-body interactions so that current flow has to be described in terms of nonequilibrium transitions between various *many-body states* (Fig. 1, right).[4–6] The multielectron master equation operates in this regime to satisfactorily explain experiments on molecular quantum dots. The transition region is complicated, as there is no obvious way to capture coherence and correlation (wave and particle aspects) within the same formalism for an open system due to the lack of a small parameter (the fine structure constant of transport, U_0/Γ being ~ 1).[7]

Efforts exist to describe both systems within the same formalism but are limited by approximations (e.g., elimination of Kondo correlations) to make such treatments tractable. However, to our knowledge, there has not been an attempt to couple two systems belonging to these diverse regimes—namely, channel electrons following wave evolution in Hilbert space and dot electrons following particle evolution in Fock space; nor has there been a pressing motivation to do so. However, such a coupling between nanoelectrons and microelectrons becomes particularly important for a side-coupled *T* geometry [Fig. 3(a)], involving ad-

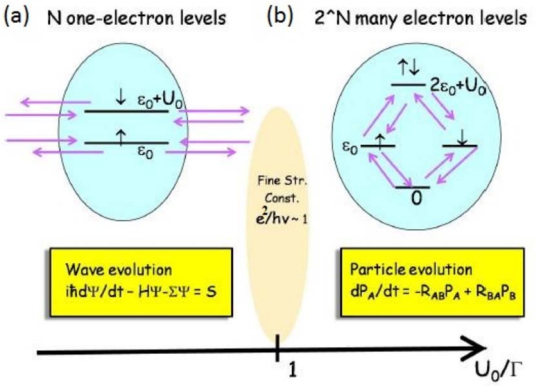

FIG. 1. (Color online) Theories for electron flow vary between (a) perturbative NEGF approaches (Ref. 2), where a single electron is added to or removed from a set of one-electron levels that incorporate interactions in mean-field and (b) multielectron master equations (Ref. 4) that take the entire electronic system between various *N*-electron many-body states. The cartoon shows the 2×2 Hilbert space vs 4×4 Fock space for two spins on a quantum dot with orbital energy ϵ_0 and Coulomb energy U_0. Γ represents the broadening of the one-electron states (or transitions between many-electron states) by coupling to the contacts, a channel, or the environment.

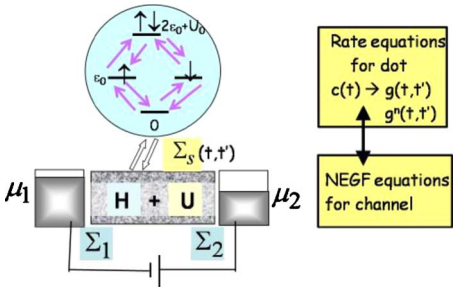

FIG. 2. (Color online) The NEGF approach consists of specifying the channel through its Hamiltonian H and potential U while capturing the contacts through self-energies $\Sigma_{1,2}$. Current is driven by the unequal electrochemical potentials $\mu_{1,2}$ in the contacts. External factors influence the channel electrons through the charging U, as well as through the scattering self-energy Σ_S. While Σ_S is traditionally calculated perturbatively, for a dot-channel coupled system we can use many-body transport equations to calculate the dot Green's functions g, g^n exactly, and use them subsequently to obtain their scattering influence in Σ_S.

sorbed dots that act as scattering states on the principle backgated transport channel. In particular, we find that through the coupling of the optical writing on the dots with electronic reading from the channel current, different physical mechanisms emerge that have bearings on detection of single charges in quantum computing. *Specifically, we propose a detection scheme for Rabi oscillations that is tunable and is readable directly from the dc*. Besides offering an exciting novel way to detect states for quantum computing, the dot-channel T junction provides an ideal system to test our coupling of Fock space and Hilbert space transport formalisms.

In this paper, we (i) present a theoretical approach to explore the time-dependent interaction between a correlated nanoscale quantum dot and a microscale backgated substrate (Fig. 2). The many-electron dynamics of the dot operators are solved directly from rate equations in their configuration (Fock) space,[4] whence we extract their one-electron scattering self-energies that drive the simpler time-dependent nonequilibrium Green's function (TDNEGF) channel equations. *The scattering matrices Σ_S are thus calculated nonperturbatively by exact diagonalizing the many-body dot Hamiltonian and projecting onto the channel one-electron subspace*. (ii) The coupling of the dot-channel transport modes creates entirely novel signatures arising from the ac optical write but detected through the dc current read. A dot coupled to a channel is known to create prominent Fano signatures through gate tunable quantum interference between parallel transport channels involving the localized dot and delocalized channel states.[9] By the incorporation of an added optical gating with a monochromatic laser pulse resonant with the dot level splittings, we can modulate the charge and spin populations and coherences in the dot. This Rabi modulation creates a *split in the Fano spectrum* [Figs. 3(b) and 4] *that can be tuned with the field strength* (power of the laser source). (iii) Many-body interactions within the dot further detune this resonant split (Fig. 5), underscoring our ability to couple interacting electrons with noninteracting and coupling the Hilbert and Fock space descriptions. (iv) The charge depletion/accumulation at the channel surface driven by a back or side gate allows us to control the Coulomb and tunnel couplings between the dot and channel modes (Fig. 7). Finally, (v) a time-resolved measurement shows prominent *beats* (Fig. 6) in the output signal if the Bohr frequencies of the dot approach the Rabi frequency, as in the case of a dot with two Zeeman split spin states. This mechanism underscores the need for doing justice to non-Markovian processes (memory) that we capture using the TDNEGF formalism.

I. FORMALISM: COUPLING FOCK SPACE WITH HILBERT SPACE

Simulating the optical write electronic read process requires a coupling of the Fock-space formalism for correlated dot dynamics[4] and the TDNEGF formalism[10] for weakly interacting quantum channel transport. For a given many-body dot Hamiltonian H_d, we first solve for the annihilation operators $c_{1,2}(t)$ using the Heisenberg equation of motion and well-known equal time anticommutation rules

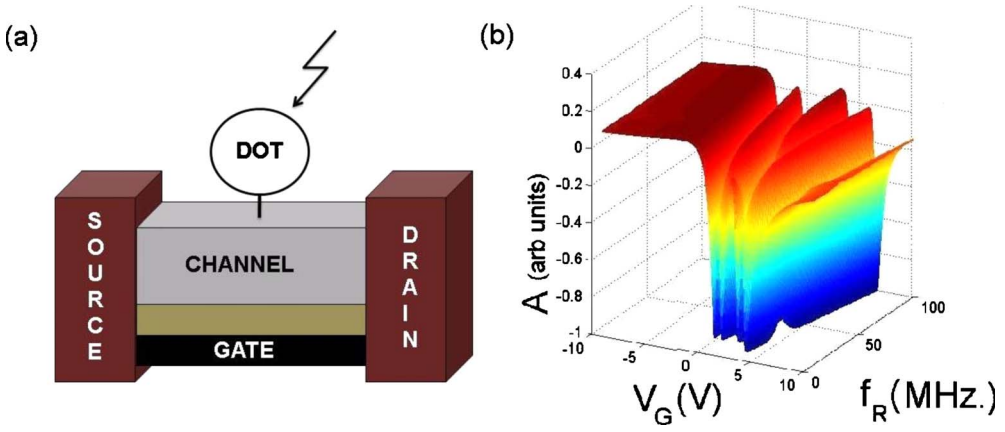

FIG. 3. (Color online) (a) Electronic detection of Rabi oscillations has relied on Pauli spin blockade between two serially coupled dots (Ref. 8). In a side-coupled geometry (typical parameters listed in Fig. 7) where the dot does not lie on the channel electron's path of propagation, we observe (b) a split of the Fano lineshape proportional to the Rabi frequencies that are tuned by the strength (power) of the incident ac field.

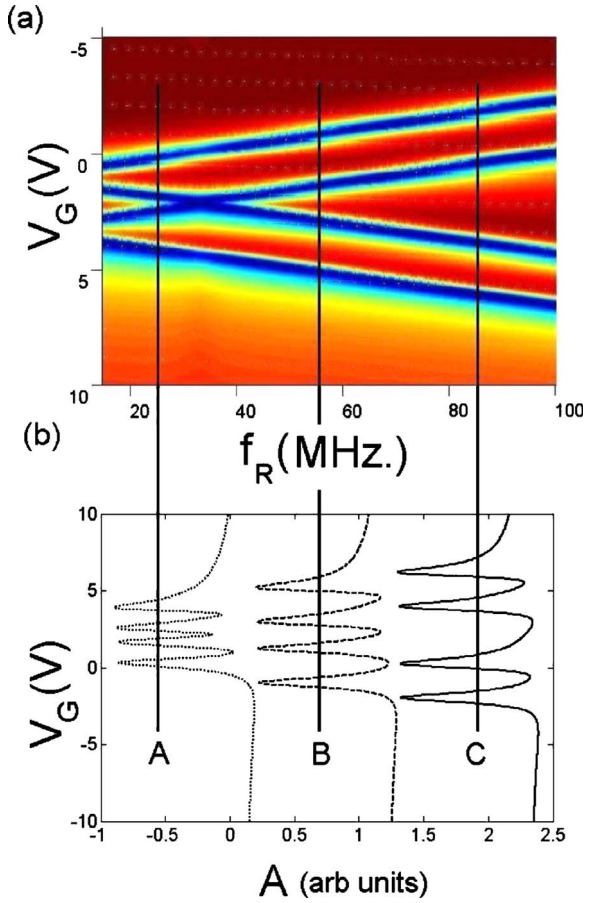

FIG. 4. (Color online) The evolving Fano lineshape at three different Rabi frequencies. Parameters: ϵ_0=0 eV, ϵ_1=0.1 eV, ΔE_Z=0.2 meV, $\gamma_L=\gamma_R$=0.01 eV, τ_c=0.25 eV, and V_d=0.001 V.

$$i\hbar\frac{\partial c_i(t)}{\partial t} = [c_i(t), H_d],$$

$$\{c_i(t), c_j^\dagger(t')\} = \delta_{ij}\delta(t-t'),$$

$$\{c_i(t), c_j(t')\} = 0, \tag{1}$$

where $[\ldots,\ldots]$ denotes the commutator and $\{\ldots,\ldots\}$ denotes the anticommutator. While this step can, in principle, be solved exactly for an isolated dot using exact diagonalization, coupling the resulting interacting electron system with continuum states in an external channel or contact serves to broaden these levels through a hybridization procedure that creates a hierarchy of Green's functions, requiring truncated at a suitable point.[11] Assuming weak dot-channel coupling and ignoring certain classes of excitations (e.g., Kondo), such a truncation arises naturally, leading to approximate expressions for the annihilation operators (we will derive explicit forms shortly). Equation (8) is a particular example of a treatment that includes interaction effects.

Once we have solved for $c_i(t)$, the dot dynamics can be captured in terms of its one-electron retarded and correlation Green's functions[2]

$$g_{ij}^R(t,t') = -i\theta(t-t')\langle\{c_i(t), c_j^+(t')\}\rangle/\hbar,$$

$$g_{ij}^n(t,t') = \langle c_j^+(t')c_i(t)\rangle, \tag{2}$$

where $\langle\ldots\rangle$ denotes a thermal average and θ is the Heaviside step function. Furthermore, the scattering of the channel states by the dot electrons can be captured using a self-energy

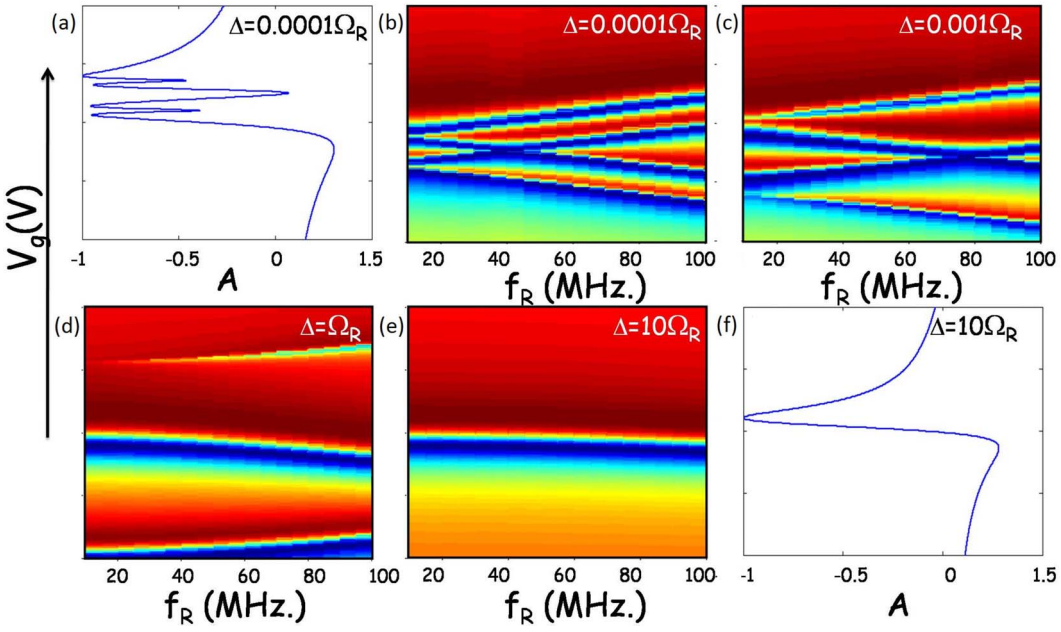

FIG. 5. (Color online) Evolution of Fano lineshape in the presence of Rabi oscillations for varying degrees of intradot Coulomb interactions that detunes the laser frequency with the dot level separation. For unmodified levels we get the Rabi split Fano shapes [(a) and (b)] (Fig. 4) while for strong Coulomb coupling/detuning we register the single level that stays coupled to the channel [(e) and (f)].

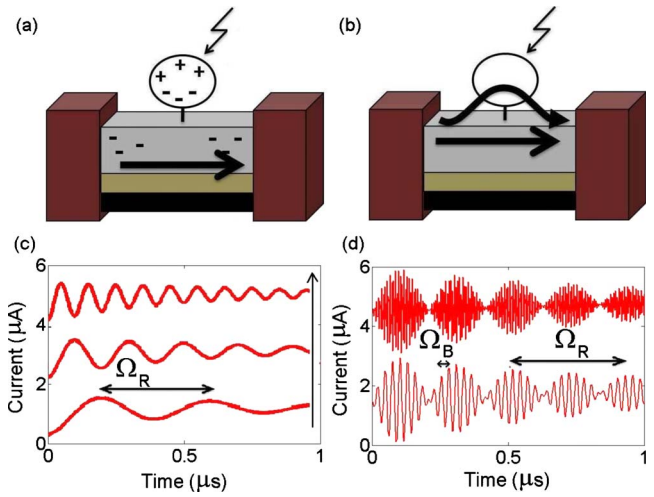

FIG. 6. (Color online) Schematic description of (a) dipolar CS and (b) short-ranged QI scattering between the dot and channel transport modes. (c) In the computed channel current for CS, the Rabi oscillations manifest themselves in the frequency shifts Ω_R =2.5 MHz, 5MHz, and 10 MHz (in direction of arrow) ($\Delta\epsilon$ =3 meV). (d) In the QI case, $\Delta\epsilon$=0.2 μeV (e.g., spin split levels in a Zeeman field), Ω_R=2.5 MHz, ϵ_{ch}=0.01 eV (channel energy), ϵ_1=0.1 eV, dot electrochemical potential μ=0 eV, dot charging energies U_1=500 μeV, U_2=50 μeV, contact broadenings $\gamma_L=\gamma_R$ =10 meV, dot-channel coupling τ_c=0.25 eV, temperature 100 mK, and decay times T_1=0.1 μs and T_2=1 μs. As the Bohr frequency Ω_B of the levels is comparable with the Rabi frequency, beats are observed in the channel current.

$$[\Sigma_s^{(R,in)}(t,t')] = \tau[g^{(R,n)}(t,t')]\tau^{\dagger}, \tag{3}$$

where $\tau=(\tau_1\tau_2)$ denotes the chemical coupling of the two dot basis states with the channel surface atoms. Since g is obtained by exact diagonalizing a many-body operator, Σ *is nonperturbative in the dot interaction potential* and is suited to handling correlation effects [e.g., Eq. (8)]. In principle, the τs could include more complicated inelastic scattering contributions such as from vibrations or spins in the dot coupled to an external thermal bath. For illustrative purposes, however, we will include only the coherent dot-channel interactions in τ, while treating the dot-bath interactions phenomenologically through additional relaxation times that we will introduce later.

In addition to these self-energies, responsible for through-bond scattering, quantum interference (QI mechanism) and the exchange of charge between the dot and the channel, there is a longer ranged Coulomb scattering (CS) mechanism that can deplete and polarize channel charges, driven by potential variations $U_1\delta n_1(t)+U_2\delta n_2(t)$, where the dot charges $n_i(t)=g_{ii}^n(t,t')$ and the Coulomb integrals U_i $=q^2\int dx\int dx'\,\phi_i^*(x)\phi_{ch}(x')/(4\pi\epsilon_r|x-x'|)$. ϵ_r denotes the material dielectric constant and $\phi_{ch}(x)$ denotes the wave function in the channel depth direction x, dictated primarily by the corresponding metal-oxide-semiconductor electrostatics. In a simple approximation (e.g., extended Hückel theory), the bond coupling τ has the form $\tau=\tau_0\int dx\int dx'\,\phi_i^*(x)\phi_{ch}(x')$ dictated by the overlap of channel and dot basis states.

The retarded and in-scattering self-energies $\Sigma^{R,in}$ and Coulomb potentials U are used to compute the transport current in the channel. In order to do justice to non-Markovian (memory) effects, we use the full TDNEGF formalism.[10,12–16] We start with the retarded and correlation channel Green's functions using the Dyson-Keldysh equations

$$G^R(t,t') = g_0(t,t') + \int dt_1dt_2g_0(t,t_1)\Sigma^R(t_1,t_2)G^R(t_2,t'),$$

$$G^n(t,t') = \int dt_1dt_2G^R(t,t_1)\Sigma^{in}(t_1,t_2)G^A(t_2,t'), \tag{4}$$

where $g_0(t,t')$ is the Green's function for the channel decoupled from the dot (but including Coulomb correlations), G^A $=(G^R)^{\dagger}$, and $\Sigma^{R,in}=\Sigma_L^{R,in}+\Sigma_R^{R,in}+\Sigma_s^{R,in}$. For contacts with broadenings $\Gamma_{L,R}(E)$ and Fermi functions $f_{L,R}(E)$, we can write $\Sigma_{L,R}^{R,in}(t,t')$ as the Fourier transforms of $\Sigma_{L,R}^{in}(E)$ $=\Gamma_{L,R}(E)f_{L,R}(E)$ and $\Sigma_{L,R}^R(E)=-i\Gamma_{L,R}(E)/2+\mathcal{H}[\Gamma_{L,R}(E)]$, where $\mathcal{H}$ denotes the Hilbert transform. From the computed Green's functions and self-energies, we can now calculate the time-dependent channel current ($\alpha=L,R$) as

$$I(t) = [I_L(t,t) - I_R(t,t)]/2,$$

$$I_\alpha(t,t') = I_\alpha^{in}(t,t') - I_\alpha^{out}(t,t'),$$

$$I_\alpha^{in}(t,t') = \frac{2q}{i\hbar}\int dt_1 Tr[\Sigma_\alpha^{in}(t,t_1)G^A(t_1,t') - \text{H.c.}],$$

$$I_\alpha^{out}(t,t') = \frac{2q}{i\hbar}\int dt_1 Tr[G^n(t,t_1)\Sigma_\alpha^A(t_1,t') - \text{H.c.}] \tag{5}$$

with $\Sigma^A=(\Sigma^R)^{\dagger}$ and H.c. the Hermitian conjugate.

Equations (2)–(5) couple the many-body quantum dynamics of the dot with the transport properties of the channel. *While the individual equations exist in the literature for the separate transport regimes, the novelty is using exact diagonalization of the dot states to compute the self-energy* [Eq. (3)], *thereby coupling the Hilbert and Fock space descriptions nonperturbatively*. Even more significant is the fact that the coupling of these formalisms yields results in the dot-channel T geometry that have important implications on direct electronic detection of Rabi oscillations. Our principle challenge at this time is to actually set up the interacting dot-channel-lead Hamiltonian and compute the dot operators $c_i(t,t')$.

II. APPLICATION: DETECTING OPTICALLY WRITTEN DOT DYNAMICS IN THE GATE TUNABLE CHANNEL CURRENT

Laser irradiating a two-level dot generates a Hamiltonian $H_{int}=E(t)d_\mu(c_1^{\dagger}c_2+\text{H.c.})$ in the $\{\phi_{1,2}\}$ dot basis. The transition dipole moment $d_\mu=q\int dx\phi_1^*(x)x\phi_2(x)$ and the laser electric field $E(t)=E_0\cos(\omega_Lt)$. Applying the Heisenberg equation for annihilation c_i operators ($i=1,2$), defining the Rabi

frequencies $\Omega_R = E_0 d_\mu/\hbar$ and Bohr frequencies $\omega_{21} = (\epsilon_2 - \epsilon_1)/\hbar$, and assuming the laser frequency is near resonance with the two-level system with a small detuning parameter $\Delta = \hbar(\omega_L - \omega_{21})$, we can invoke the rotating wave approximation (RWA). The algebra can be simplified into a compact, elegant form

$$\begin{pmatrix} c_1(t) \\ c_2(t) \end{pmatrix} = \bar{U}(t) \begin{pmatrix} c_1 \\ c_2 \end{pmatrix},$$

$$\bar{U}(t) = \exp[-i(H_0 - \hbar\Delta/2)t/\hbar + i\vec{\sigma}\cdot\hat{n}\Omega t/2], \tag{6}$$

where H_0 is the isolated dot Hamiltonian with eigenvalues $\epsilon_{1,2}$, $\vec{\sigma}$ is the Pauli spin vector, while the unit vector $\hat{n} = (\Omega_R, 0, \Delta)/\Omega$ with $\Omega = (\Delta^2 + \Omega_R^2)^{1/2}$. The explicit solutions for the c_i operators then lead to the Green's functions for the dot using Eq. (2)

$$[g^R(t,t')] = -\frac{i}{\hbar}\theta(t-t')\bar{U}(t)\bar{U}^+(t')e^{-(t+t')/T},$$

$$[g^n(t,t')] = \bar{U}(t)\rho\bar{U}^+(t')e^{-(t+t')/T}, \tag{7}$$

where ρ is the density matrix of the isolated dot with diagonal entries given by the equilibrium occupancies of the dot states. The g's in turn yield the scattering term $\Sigma_s(t,t')$ for the QI mechanism and the charge polarization δn for the CS mechanism. Before we proceed further, let us discuss the rationale behind our phenomenological treatment of environmental fluctuations through the decay constants $T_{1,2}$.

III. APPROXIMATIONS: TREATMENT OF DEPHASING AND INTRADOT INTERACTIONS

While the challenge of our formalism is the employment of many-body dot Green's functions [Eq. (2)] to drive the one electron channel Green's functions [Eq. (4)], our main approximation at this stage is the use of the *isolated* dot Green's functions to compute its scattering influence Σ_S. While we can easily work around this limitation for weak dot-channel coupling τ, the absence of significant interactions in the channel (and our deliberate ignorance of Kondo correlations) means that the influence of stronger coupling can be easily incorporated, principally as a broadening $\Gamma_{1,2}$ of the states given by Fermi's golden rule, $\Gamma_{1,2} = 2\pi|\tau_{1,2}|^2\rho_0$, with ρ_0 being the known channel density of states. This means that we can continue to use the isolated dot equations while simply renormalizing the dot levels as $\tilde{\epsilon}_{1,2} \approx \epsilon_{1,2} - i\Gamma_{1,2}/2$ (any energy dependence of $\Gamma_{1,2}$ would create an additional shift in the energies given by a simple Hilbert transform). What is harder to include is the broadening of the dot states by coupling with the external environment, such as a thermal bath, since that depends on microscopic details of the underlying broadening mechanism. Lacking specific knowledge of these environmental decoherences, we choose to include them in Eq. (7) using a phenomenological decay parameter T, amounting to a diagonal relaxation time T_1 and an off-diagonal decoherence time T_2. These terms are necessary to capture the physics of the electrons entering and leaving the dot.

This inclusion in Eq. (7) as an exponential term can be rigorously derived. One needs to start with the many-body Hamiltonian coupling the dot with the environment, which looks like $H = \epsilon_0 c^\dagger c + \Sigma_k \epsilon_k c_k^\dagger c_k + \Sigma_k(\tau_k c^\dagger c_k + \tau_k^* c_k^\dagger c)$ where c_k is the environmental degree of freedom and c is the dot variable. The result looks like an open boundary Schrödinger wave equation where the self-energy $\Sigma(t,t') = \Sigma_k|\tau_k|^2 e^{-i\epsilon_k(t-t')/\hbar}$ and the source $S(t) = \Sigma_k \tau_k c_{k0} e^{-i\epsilon_k t/\hbar}$. If we ignore the energy dependence of Σ, which is consistent with a phenomenological description of the environmental degrees of freedom, we can show that $c(t) = c_0 e^{-i(\epsilon_0+\Sigma)t/\hbar} + \frac{1}{i\hbar}\int dt' S(t') e^{-i(\epsilon_0+\Sigma)(t-t')/\hbar}$. Using Eq. (2) we can thus calculate the Green's functions exactly, with the decaying exponential terms. It is also straightforward to show that the above c operators with the exponents exactly satisfy the equal time anticommutation relation.

The main strength of our model is the nonperturbative evaluation of the scattering matrices and the resulting coupling of the interacting dot response function with noninteracting transport equations in the underlying channel [Eqs. (1)–(3)]. We are thus completely flexible in our ability to handle intradot interactions. For instance, we could directly use exact diagonalization to evaluate our gs (e.g., using the 4×4 many-body states in Fig. 2 right). Alternately, we can build interactions into the quantum dot response functions by standard diagrammatic techniques,[11] for larger multilevel dots where exact diagonalization may prove impractical. For example, we can include an on-site Hubbard term U_d on the dot by evolving the dot Green's functions with an equation of motion technique and then truncating the hierarchy of dot equations within a "local moment" approximation,[11] yielding a probability weighted result

$$g^{R,n}_{\sigma,int}(t,t') \approx (1 - \langle n_{\bar{\sigma}}(t')\rangle) g^{R,n}_{\sigma}(t,t') + \langle n_{\bar{\sigma}}(t')\rangle g^{R,n}_{\sigma}(t,t') e^{-iU_d(t-t')} \tag{8}$$

for a given spin σ and its inverse $\bar{\sigma}$. This Coulomb interaction includes correlation effects such as self-interaction correction so that the effect on a specific spin state depends the occupancy of the other spin states. Higher order terms can generate further interactions, such as high-temperature Kondo correlations,[11] possibly even extended to multiple orbitals.[17] We will now see how the combination of memory effects, coherence and correlation effects adds incredible richness to the spectrum of the dot scattering states as detected in the channel current.

IV. RESULTS: DETECTING RABI OSCILLATIONS THROUGH STATIC (dc) CHANNEL CONDUCTANCE

In the past, electronic detection of Rabi oscillations relied on Pauli spin blockade between two serially coupled dots and its effect on the time-dependent current.[8] In a parallel transport geometry, however, the channel electrons are not Pauli blocked by the side coupling, as the dot does not lie on the channel electron's path of propagation. The coupling of paths can occur through the long-ranged Coulomb terms U sitting in g_0 that deplete the channel electrons [Fig. 6(a)] and

generate time-resolved transport signatures [Fig. 6(c)] reminiscent[8] of spin blockade. However, a much more interesting mechanism avails itself in this specific side-coupled T geometry, where lateral transport paths through the channel continua and the localized dot states interfere quantum mechanically through direct chemical bonding between the dot and the channel surface atoms [Fig. 6(b)], generating a phase-coherent Fano interference directly in the dc current characteristics. *In other words, we can use a side-coupled geometry to detect Rabi oscillations directly from the dc conductance spectrum.*

While Fano signatures are common in quantum dots,[9] in the dual optical-electronic gated system described here *the Fano lineshape gets convolved with the Rabi signatures impressed upon the dot by the ac field*. Expanding and simplifying Eq. (7), we see that the Rabi-Fano interaction manifests itself directly in the dc spectrum as a field-tunable split in the Fano lineshape (Fig. 4).

We can readily include Coulomb correlations in our model, say by using Eq. (8). Self-interaction correction will make one level repel the other through a mutual Coulomb potential. If the laser frequency is resonantly tuned to the bare level splitting, increasing Coulomb corrections will increase the detuning Δ. As Fig. 5 suggests, the detuning will spread out the spectral weights of the Rabi-split Fano. The spectral weights of the two Rabi split levels ($\pm$ for $i=1,2$, respectively) and thereby the change in channel spectral function can be obtained to yield the Rabi modulated Fano lineshape. This can be done numerically using the Crank-Nicholson technique to solve the time-dependent evolution of the wave functions exactly. We confirm that this matches the analytical results we obtain invoking the small Δ RWA. To do this we work out the Green's function for a combined dot-channel system coupled through τ, and then partition the matrix to extract the effect of the coupling on the channel electrons.[18] We can thus find an expression for the Rabi modulated channel Green's function with finite detuning, along with the corresponding spectral function A which determines its density of states and thus its conductance spectrum

$$g_{ii}(E) \approx \frac{1-\Delta/\Omega}{E-\epsilon_1+i\gamma_1 \pm \hbar(\Delta+\Omega)/2} + \frac{1+\Delta/\Omega}{E-\epsilon_1+i\gamma \pm \hbar(\Delta-\Omega)/2},$$

$$\delta A = g_{ch}\left[1-\frac{(q+\xi)^2}{\xi^2+1}\right], \tag{9}$$

where g_{ch} is the bare channel Green's function, q is the phase angle of the channel, and ξ is the phase angle of the dot,[18] extracted from the expression above for g_{ii}. The increasing detuning will lead ultimately to the bare Fano lineshapes between the dot and channel states unmodified by the Rabi oscillations. The result shown in Fig. 5 required the incorporation of correlation effects (in this case, self-interaction correction translated to an overall detuning), into a traditional NEGF treatment of conductance and Fano interference.

V. RESULTS: DETECTING RABI OSCILLATIONS IN THE TIME-DEPENDENT CHANNEL CURRENT

Further physics is unearthed by looking at the time-resolved current. The usual Rabi modulation of the current can be captured using Coulomb Blockade [Figs. 6(a) and 6(c)]. For a serially coupled dot array, the modulation of the current arose from the distinct potentials acting on different spins (spin blockade). In the Coulomb blockade analog likewise, it is critical to have different Coulomb repulsions from the different levels. The Coulomb repulsive term can be written as $U_1\delta n_1+U_2\delta n_2=U_{av}\delta n_{av}+\Delta U\delta\mu$, where $U_{av}=(U_1+U_2)/2$ and $\delta n_{av}=(\delta n_1+\delta n_2)/2$ are the averages while $\Delta U=(U_1-U_2)$ is the differential charging energy between the dot levels and $\delta\mu=(\delta n_1-\delta n_2)$ is the net dipole on the dot. A Rabi induced reorganization of the charges on the dot simply alters the dipole moment that can only scatter the channel if there is a differential charging ΔU on the dot. In contrast, direct Coulomb scattering by the average Coulomb potential U_{av} can only occur if charge actually enters or leaves the channel through the Σ^{in} terms (i.e., effectively, the broadenings Γ).

The usefulness of the side-coupled geometry arises from the employment of through bond coupling and interference between parallel transport channels as an alternate means for transmitting the Rabi signatures to the channel current. While this shows up as a field-tunable split in the dc conductance (Fig. 4), they also manifest themselves in the time-resolved current as field-tunable beats [Fig. 6(d)], amplified when the Rabi frequency approaches the intrinsic Bohr frequencies in the dot to which the laser is resonantly tuned. The origins of the dc and ac Rabi signatures however are patently different—the spectral modifications in Fig. 4 arise from g^R while the temporal beats and memory effects in Fig. 6 arise from g^n. Expanding Eq. (7), we find that the sum of the diagonal terms $g^n_{11}+g^n_{22}$ in the expression for Σ^{in} is independent of the average time index $T=(t+t')/2$ so that any time modulation arises essentially out of the off diagonal sum $g^n_{12}+g^n_{21}$. In the absence of memory effects (i.e., setting $t_d=t-t'=0$), this sum is proportional to $[\sin\Omega T \sin(\epsilon_1-\epsilon_2)T](f_1-f_2)$ which generates the observed beats between the Rabi and Bohr frequencies. Non-Markovian corrections built into the TDNEGF formula provide an additive correction proportional to $[\sin\Omega t_d/2 \cos(\epsilon_1-\epsilon_2)T](f_1+f_2)$.

Dipolar Rabi frequencies are typically much smaller than electronic state spacings but the two do approach each other in their spintronic analog where the tunnel coupling is replaced by the Heisenberg exchange between the spin bits and the channel electrons[19] with the Zeeman splitting of spin states often ending up being comparable to the electron spin resonance frequency. Capturing these beats correctly requires careful attention to memory effects that our TDNEGF model incorporates.

VI. PARAMETER DEPENDENCE AND TUNABILITY

Electronic readout of qubits is crucial for integrating quantum-computing paradigms with a solid-state architecture compatible with present day microelectronics. It also pro-

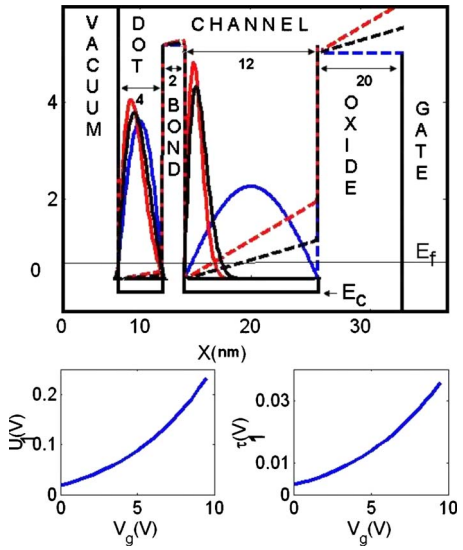

FIG. 7. (Color online) Top: band lineup and eigenstates for dot-channel geometry [shown in Fig. 3(a)] for three representative gate voltages at V_g=0 V (blue line), 2 V (black line), 3.2 V (red line) Parameters: ϵ_γ=1.7, τ_0=25 μeV (Ref. 21). The backgate to the right of the figure can be used to tune the electron density and wave function at the channel surface, thereby controlling both the Coulomb integral U_1 (bottom left) and the bond coupling parameters τ_1 (bottom right) between the channel surface and the lowest electronic state of the dot.

vides the possibility of real-time detection of the dot's molecular "fingerprints."[20] One can engineer the couplings at a molecular level through synthetic chemistry or by gate tuning. The use of multiple gates would allow us to independently scan the location of the channel/dot states and also control the dot-channel coupling.

Figure 7 shows our ability to tune the charging energy $U_1\delta n_{11}$ and the coupling τ_1 for the dot ground state, in other words, controlling the parameters for CS and QI, respectively. The former depends ultimately on the charge density at the interface while tuning the dot-channel wave function overlap further modulates U_1 and τ_1. By using a backgate, we can deplete or enhance the surface electron density and also control the wave function overlap through a Stark shift of the channel states. In our example, we considered a 10 nm dot coupled to a 12-nm-deep channel sitting on a 20 nm oxide through a 2 nm interfacial bond (e.g., a linker molecule). As the backgate voltage is cranked up, the overall band-diagram shifts due to the overall electrostatics given by the individual component geometries and dielectric constants. The smooth curves show the ground-state eigenfunctions in each well, and these get polarized as the potentials tilt, generating a Stark shift that alters the overlap between $\phi_{ch}(x)$ and $\phi_i^*(x)$. The altered overlap changes the U_1 and τ_1 parameters, calculated using the simplified expressions described in the paragraphs preceding Eq. (4).

VII. SUMMARY

In a side-coupled geometry involving noninteracting channel electrons scattering off of interacting dot electrons, we predict a slew of signatures including a Rabi induced splitting of the dc Fano lineshape, as well as beats in the time-dependent current due to the interaction between Rabi and Bohr frequencies. While this is potentially significant for the electronic detection of single charges, capturing this physics correctly required a marriage of formalisms that has not been attempted thus far, to the best of our knowledge. Specifically, we needed *memory effects* within the TDNEGF formalism to capture the beats in the time-dependent current (Fig. 6). We needed to pay attention to *quantum coherence* in the channel G matrices to capture the Fano lineshapes arising out of quantum interference between dot and channel transport states (Fig. 4). Finally, we also needed to do justice to *many-body correlation physics* in the dot g terms to capture the physics of self-interaction correction that generates a detuning on the Fano lineshape (Fig. 5). The resulting plots bear rich spectral signatures of the dot-channel interaction, and provide a viable route toward optically writing information onto the dot electrons and transducing their dynamics electronically into the gate tunable channel current.

ACKNOWLEDGMENTS

We would like to thank Keith Williams, Robert Weikle, and Lloyd Harriott for useful discussions. This work was supported by DARPA-AFOSR, NSF-NIRT, and NSF-CAREER awards. K. Walczak is grateful to NRC/NRL for support.

[1] M. Xiao, I. Martin, E. Yablonovitch, and H. W. Jiang, Nature (London) **430**, 435 (2004).
[2] S. Datta, *Quantum Transport: Atom to Transistor*, 2nd rev. ed. (Cambridge University Press, Cambridge, 2005).
[3] P. S. Damle, A. W. Ghosh, and S. Datta, Phys. Rev. B **64**, 201403 (2001).
[4] B. Muralidharan, A. W. Ghosh, and S. Datta, Phys. Rev. B **73**, 155410 (2006).
[5] B. Muralidharan, A. W. Ghosh, S. Pati, and S. Datta, IEEE Trans. Nanotechnol. **6**, 536 (2007).
[6] B. Muralidharan, L. Siddiqui, and A. W. Ghosh, J. Phys.: Condens. Matter **20**, 374109 (2008).
[7] B. Muralidharan, A. W. Ghosh, and S. Datta, Mol. Simul. **32**, 751 (2006).
[8] F. H. L. Koppens, C. Buizert, K. J. Tielrooij, I. T. Vink, K. C. Nowack, T. Meunier, L. P. Kouwenhoven, and L. M. K. Vandersypen, Nature (London) **442**, 766 (2006).
[9] A. C. Johnson, C. M. Marcus, M. P. Hanson, and A. C. Gossard, Phys. Rev. Lett. **93**, 106803 (2004).
[10] A.-P. Jauho, N. S. Wingreen, and Y. Meir, Phys. Rev. B **50**, 5528 (1994).
[11] Y. Meir, N. S. Wingreen, and P. A. Lee, Phys. Rev. Lett. **66**,

3048 (1991).
[12] H. Haug and A.-P. Jauho, *Quantum Kinetics in Transport and Optics of Semiconductors* (Springer-Verlag, Berlin, 1996).
[13] Y. Zhu, J. Maciejko, T. Ji, H. Guo, and J. Wang, Phys. Rev. B **71**, 075317 (2005).
[14] D. Hou, Y. He, X. Liu, J. Kang, J. Chen, and R. Han, Physica E **31**, 191 (2006).
[15] S. Datta, *Nanodevices and Maxwell's Demon*, Lecture Notes in Nanoscale Science and Technology (Springer, New York, 2008), Vol. 2, Part II, pp. 59–81.
[16] S. Datta, arXiv:cond-mat/0603034 (unpublished).
[17] A. Levy Yayati and M. Büttiker, Phys. Rev. B **52**, R14360 (1995).
[18] A. W. Ghosh, *Electronics with Molecules*, Semiconductor Science and Technology, edited by P. Bhattacharya, R. Fornari, and H. Kamimura (Elsevier, in press), Vol. 1.
[19] A. R. Stegner, C. Boehme, H. Huebl, M. Stutzmann, K. Lips, and M. S. Brandt, Nat. Phys. **2**, 835 (2006).
[20] S. Vasudevan, F. Tseng, and A. W. Ghosh (unpublished).
[21] W. G. van der Wiel, T. Fujisawa, S. Tarucha, and L. P. Kouwenhoven, Jpn. J. Appl. Phys. **40**, 2100 (2001).